J Electr Eng Technol.2018; 13(1): 298-306
http://doi.org/10.5370/JEET.2018.13.1.298

ISSN(Print) 1975-0102
ISSN(Online) 2093-7423

Harmonic Analysis of a Modular Multilevel Converter Using Double Fourier Series

Ngoc-Thinh Quach*, Sang Heon Chae*, Jin Hong Ahn* and Eel-Hwan Kim†

Abstract – This paper presents a harmonic analysis of the modular multilevel converter (MMC) using a double Fourier series (DFS) algorithm. First, the application of DFS for harmonic calculation in the MMC is made by considering the effect of arm inductor. The analytical results are then confirmed by comparing with the simulation results of using the fast Fourier transform (FFT) algorithm. Finally, distribution of harmonics and total harmonic distortion (THD) in the MMC will be analyzed in three cases: harmonics versus number of levels of MMC, harmonics versus total switching frequency and harmonics versus modulation index. The simulation results are performed in the PSCAD/EMTDC simulation program in order to verify the analytical results obtained by Matlab programming.

Keywords: Double Fourier series, Fast Fourier transform, Harmonic analysis, Modular multilevel converter, Total harmonic distortion

1. Introduction

The modular multilevel converter (MMC) has been developed for medium and high voltage applications in recent years. The advantages of the MMC over the conventional voltage source converter (VSC) are low total harmonic distortion (THD), high efficiency and high capacity [1, 2]. The operation principles of MMC have been studied by many authors over the world [3-5]. In [6]-[9], the authors have presented the modulation methods for the MMC. Among the SPWM methods, the phase-shifted PWM method is known as a simple modulation method because the generation of gating signals is similar to the case of conventional VSC. Although in low THD, the MMC also injects the harmonics into AC side of the power system. Moreover, the distribution of harmonics changes according to the operating condition. An analysis of harmonics is quite complex and it is often done by using fast Fourier transform (FFT) algorithm [10]. This method offers the benefits of expediency and reduces mathematical effort, but requires considerable computing capacity at a higher carrier frequency. Besides, the FFT often causes a slight error to the obtained results because this method is quite sensitive to both the time resolution of simulation and the periodicity of the overall waveform. In contrast, an analytical method which can calculate the harmonics with a higher precision has been introduced by Bennett [11] for communication applications. This method is named by a double Fourier series (DFS) algorithm. During last years, the application of DFS for analyzing harmonics in the VSC topologies, such as single-phase VSC, three-phase VSC, diode-clamped multilevel converter and cascaded multilevel converter, has been researched by many authors [7, 10, 12-15]. In [7], the authors have presented a harmonic analysis of general multilevel converters using the DFS. Besides, a DFS expansion has been also used to determine how the fundamental and low-order harmonics interact with carrier to produce the low and high order frequencies in the PWM VSC output voltage [12]. In [13], the DFS has been applied for calculating the harmonic and interharmonic currents generated by the three-phase converter under unbalanced supply voltages. The DFS can be also used to calculate harmonics in a H-Bridge converter with dead time [15]. There is still no study on application of DFS for the MMC although the MMC is a promising multilevel converter topology in the near future; therefore, a harmonic analysis of the MMC is necessary.

This paper presents a harmonic analysis of the MMC using the DFS algorithm. The objective is to determine the distribution of harmonics as well as the THD in the MMC. To do so, the application of DFS for calculating harmonics in the MMC is first made by considering the effect of arm inductor. Then, the analytical results of using the DFS are confirmed by comparing with the simulation results of using the FFT. Finally, the distribution of harmonics as well as the THD in the MMC will be analyzed in three cases: harmonics versus number of levels of MMC, harmonics versus total switching frequency and harmonics versus modulation index.

The rest of this paper is as follows. Section 2 presents the structure and operation of the MMC briefly. The application of DFS for analyzing harmonics in the MMC is explained in Section 3. Section 4 shows the simulation results and discussion. Section 5 draws the conclusions.

† Corresponding Author: Dept. of Electrical Engineering, Jeju National University, Korea. (ehkim@jejunu.ac.kr)
* Dept. of Electrical Engineering, Jeju National University, Korea. (ngocthinh@ctu.edu.vn,{chae, jinhong3215}@jejunu.ac.kr)
Received: October 20, 2016; Accepted: October 7, 2017

2. Modular Multilevel Converter

The basic structure of the MMC is shown in Fig. 1. The MMC is created by six arms which are arranged as illustrated in Fig. 1(a). Each arm has a total of N submodules (SMs) connected in series and a series inductor. Two arms in the same leg comprise a phase unit. Each SM is a half-bridge cell that consists of two IGBTs, two anti-parallel diodes and a capacitor, as seen in Fig. 1(b). The AC side of the MMC is connected to the unity grid through a Y-Δ three-phase transformer.

If there are N SMs per each arm, the number of levels in output voltage will be $N + 1$. The MMC with N+1 levels in output voltage is called by N+1-level MMC. Each level is generated according to the number of SMs in the on-state in the upper and lower arms. At any instant, N SMs have to be in the on-state and N SMs have to be in the off-state in each phase unit. To turn the IGBTs on and off in each SM, the PWM methods are used. One of them is the SPWM method in which a sinusoidal reference signal is compared with carrier waveforms to generate the gating signals for the IGBTs. The MMC with N SMs per arm requires N carrier waveforms. Depending on the arrangement of the carrier waveforms, the SPWM method can be classified into categories as: phase-shifted PWM (PS-PWM), phase disposition PWM (PD-PWM), phase opposite disposition PWM (POD-PWM), alternative phase opposite disposition PWM (APOD-PWM) and saw-tooth rotation PWM (STR-PWM).

In this analysis, the PS-PWM method will be applied for the MMC as shown in Fig. 2 because it is a simple modulation method. The PS-PWM method consists of N carrier waveforms which have the same frequency and the peak-to-peak amplitude, but there is a phase shift between two adjacent carrier waveforms. This phase shift is given by

$$\varphi = \frac{2\pi}{N} \ (rad) \tag{1}$$

or the arrangement of the carrier waveforms can be explained by the phase shift between the first carrier waveform and Nth carrier waveform as follows.

$$\varphi_i = \frac{2\pi(i-1)}{N} \ (rad) \quad i = 1,2,3,...,N \tag{2}$$

The PS-PWM method has the switching frequency on each IGBT equal to the carrier frequency, f_c. In other words, total switching frequency, f_{ct}, of N SMs in each arm will be equal to $N.f_c$ ($f_{ct} = N.f_c$).

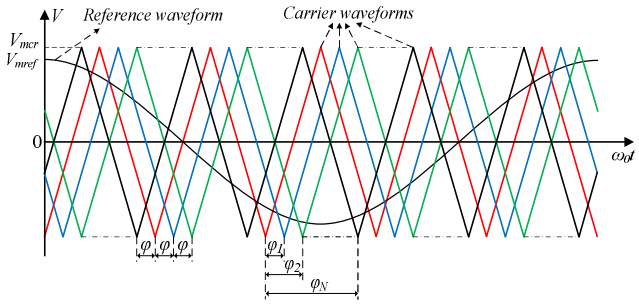

Fig. 2. Phase-shifted PWM method for the MMC

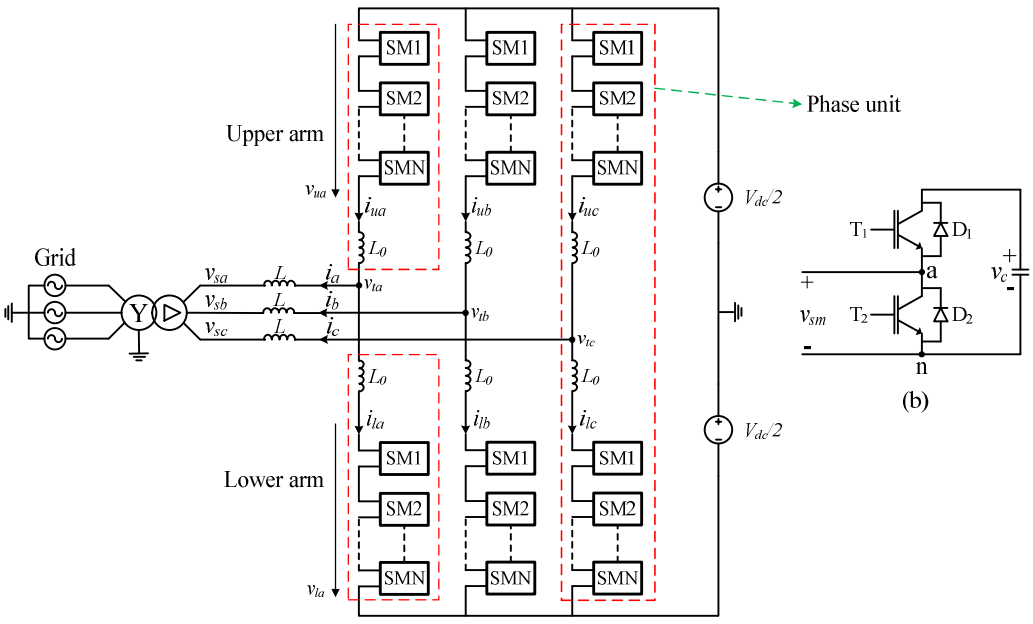

Fig. 1. Configuration of the MMC: (a) Circuit diagram, (b) Submodule

3. Harmonic Analysis with Double Fourier Series

From the DFS theory, any periodic function *f(t)* in the 3-D space *xyz* can be expressed as

$$\begin{aligned} z &= f(t) = f(x,y) \\ &= \frac{A_{00}}{2} + \sum_{n=1}^{\infty}\left[A_{0n}\cos ny + B_{0n}\sin ny\right] \\ &\quad + \sum_{m=1}^{\infty}\left[A_{m0}\cos my + B_{m0}\sin my\right] \\ &\quad + \sum_{m=1}^{\infty}\sum_{\substack{n=-\infty \\ (n\neq 0)}}^{\infty}\left[A_{mn}\cos(mx+ny) + B_{mn}\sin(mx+ny)\right] \end{aligned} \tag{3}$$

where

$$\overline{C}_{mn} = A_{mn} + jB_{mn} = \frac{1}{2\pi^2}\int_{-\pi}^{\pi}\int_{-\pi}^{\pi} f(x,y)e^{j(mx+ny)}dxdy \tag{4}$$

$$y = \omega_0 t + \theta_0 \tag{5}$$

$$x = \omega_c t + \theta_c \tag{6}$$

ω_0 and ω_c are angular frequencies of the fundamental output waveform and the carrier waveform, respectively; θ_0 and θ_c are initial phase angles of the fundamental output waveform and the carrier waveform, respectively, and they are set to zero in this paper ($\theta_0 = \theta_c = 0$).

In this paper, the DFS is used to analyze the harmonics in PWM voltage source converter. Fig. 3 illustrates the generation of the double-edge modulated voltage train of a single-phase PWM converter (Submodule in Fig. 1(b)) with DFS and conventional PWM methods. It is demonstrated that these two methods are equivalent in generating the PWM output voltage waveform.

To obtain a sinusoidal output, the reference waveform has the form as

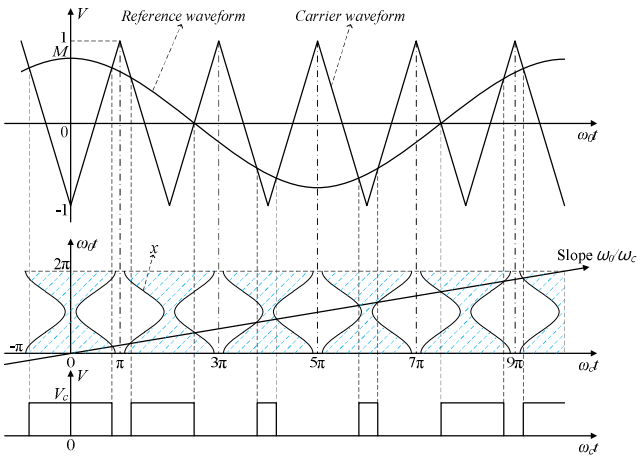

Fig. 3. Conventional PWM method and 2-D model of DFS (ω_0/ω_c = 1/5)

$$v_{ao}^{*} = M\cos y \tag{7}$$

where M is the modulation index.

The integration limits in (4) can be expressed as

+ Lower limit:

$$x = 2\pi i - \frac{\pi}{2}(1 + M\cos\omega_0 t) \qquad i = 0,1,2,...,\infty \tag{8}$$

+ Upper limit:

$$x = 2\pi i + \frac{\pi}{2}(1 + M\cos\omega_0 t) \qquad i = 0,1,2,...,\infty \tag{9}$$

Substituting these integration limits into (4), we can get

$$A_{mn} + jB_{mn} = \frac{1}{2\pi^2}\int_{-\pi}^{\pi}\int_{-\frac{\pi}{2}(1+M\cos\omega_0 t)}^{\frac{\pi}{2}(1+M\cos\omega_0 t)} V_c e^{j(mx+ny)}dxdy \tag{10}$$

where V_c is the capacitor voltage of the SM and it is determined by

$$V_c = \frac{V_{dc}}{N} \tag{11}$$

Solving (10) and then substituting into (3), the harmonic solution for a double-edge modulated voltage train of the single-phase PWM converter, $v_{sm}(t)$, can be achieved as follows.

$$\begin{aligned} v_{sm}(t) &= \frac{V_c}{2} + \frac{V_c}{2}M\cos\omega_0 t \\ &\quad + \frac{2V_c}{\pi}\sum_{m=1}^{\infty}\frac{1}{m}J_0\left(m\frac{\pi}{2}M\right)\sin\left(m\frac{\pi}{2}\right)\cos(m\omega_c t) \\ &\quad + \frac{2V_c}{\pi}\sum_{m=1}^{\infty}\sum_{\substack{n=-\infty \\ n\neq 0}}^{\infty}\frac{1}{m}J_n\left(m\frac{\pi}{2}M\right)\sin\left([m+n]\frac{\pi}{2}\right)\cos(m\omega_c t + n\omega_0 t) \end{aligned} \tag{12}$$

where $J_0(.)$ and $J_n(.)$ are the Bessel functions.

Eq. (12) shows the solution for the output voltage of the SM. As mentioned before, each arm of the MMC is created by N SMs connected in series and a series arm inductor. Therefore, if the voltage drop on arm inductor is ignored, the lower arm voltage of the phase A, $v_{la}(t)$, will be a sum of the output voltages of N SMs per arm.

$$\begin{aligned} v_{la}(t) &= \sum_{i=1}^{N} v_{sm}^{i}(t) = \frac{NV_c}{2} + \frac{NV_c}{2}M\cos\omega_0 t \\ &\quad + \frac{2V_c}{\pi}\sum_{m=1}^{\infty}\frac{1}{m}J_0\left(m\frac{\pi}{2}M\right)\sin\left(m\frac{\pi}{2}\right)\sum_{i=1}^{N}\cos\left(m\left[\omega_c t + \frac{2\pi(i-1)}{N}\right]\right) \\ &\quad + \frac{2V_c}{\pi}\sum_{m=1}^{\infty}\sum_{\substack{n=-\infty \\ n\neq 0}}^{\infty}\frac{1}{m}J_n\left(m\frac{\pi}{2}M\right)\sin\left([m+n]\frac{\pi}{2}\right)\sum_{i=1}^{N}\cos\left(m\left[\omega_c t + \frac{2\pi(i-1)}{N}\right] + n\omega_0 t\right) \end{aligned} \tag{13}$$

For all $m \neq kN$ (k = 1, 2,..., ∞), Eq. (13) can be rewritten as

$$\begin{aligned} v_{la}(t) &= \frac{NV_c}{2} + \frac{NV_c}{2} M \cos\omega_0 t \\ &+ \frac{2V_c}{\pi} \sum_{m=1}^{\infty} \frac{1}{m} J_0\left(Nm\frac{\pi}{2}M\right) \sin\left(Nm\frac{\pi}{2}\right) \cos\left(Nm\omega_c t\right) \\ &+ \frac{2V_c}{\pi} \sum_{m=1}^{\infty} \sum_{\substack{n=-\infty \\ n\neq 0}}^{\infty} \frac{1}{m} J_n\left(Nm\frac{\pi}{2}M\right) \sin\left(\left[Nm+n\right]\frac{\pi}{2}\right) \\ &\cos\left(Nm\omega_c t + n\omega_0 t\right) \end{aligned} \tag{14}$$

From Fig. 1, the output voltage of phase A, $v_a(t)$, can be achieved by ignoring the dc component in (14) as

$$\begin{aligned} v_a(t) &= \frac{NV_c}{2} M \cos\omega_0 t \\ &+ \frac{2V_c}{\pi} \sum_{m=1}^{\infty} \frac{1}{m} J_0\left(Nm\frac{\pi}{2}M\right) \sin\left(Nm\frac{\pi}{2}\right) \cos\left(Nm\omega_c t\right) \\ &+ \frac{2V_c}{\pi} \sum_{m=1}^{\infty} \sum_{\substack{n=-\infty \\ n\neq 0}}^{\infty} \frac{1}{m} J_n\left(Nm\frac{\pi}{2}M\right) \sin\left(\left[Nm+n\right]\frac{\pi}{2}\right) \\ &\cos\left(Nm\omega_c t + n\omega_0 t\right) \end{aligned} \tag{15}$$

Similarly, the output voltage of the phase B, $v_b(t)$, will be expressed as

$$\begin{aligned} v_b(t) &= \frac{NV_c}{2} M \cos\left(\omega_0 t - \frac{2\pi}{3}\right) \\ &+ \frac{2V_c}{\pi} \sum_{m=1}^{\infty} \frac{1}{m} J_0\left(Nm\frac{\pi}{2}M\right) \sin\left(Nm\frac{\pi}{2}\right) \cos\left(Nm\omega_c t\right) \\ &+ \frac{2V_c}{\pi} \sum_{m=1}^{\infty} \sum_{\substack{n=-\infty \\ n\neq 0}}^{\infty} \frac{1}{m} J_n\left(Nm\frac{\pi}{2}M\right) \sin\left(\left[Nm+n\right]\frac{\pi}{2}\right) \\ &\cos\left(Nm\omega_c t + n\left[\omega_0 t - \frac{2\pi}{3}\right]\right) \end{aligned} \tag{16}$$

The line-to-line output voltage between phase A and phase B, $v_{ab}(t)$, of the MMC is calculated as

$$v_{ab}(t) = v_a(t) - v_b(t) \tag{17}$$

Substituting (15) and (16) into (17) and rearranging, we can get

$$\begin{aligned} v_{ab}(t) &= \frac{\sqrt{3}NV_c}{2} M \cos\left(\omega_0 t + \frac{\pi}{6}\right) + \\ &+ \frac{4V_c}{\pi} \sum_{m=1}^{\infty} \sum_{\substack{n=-\infty \\ n\neq 0}}^{\infty} \frac{1}{m} J_n\left(Nm\frac{\pi}{2}M\right) \sin\left(\left[Nm+n\right]\frac{\pi}{2}\right). \\ &.\sin\left(\frac{n\pi}{3}\right) \cos\left(Nm\omega_c t + n\omega_0 t - \frac{n\pi}{3} + \frac{\pi}{2}\right) \end{aligned} \tag{18}$$

From (18), there are some notices for the line-to-line output voltage as follows.

+ There are no baseband harmonics.
+ The carrier harmonics don't appear because they are the same for all phases.
+ The sideband harmonics with even combinations of $Nm + n$ and triplen sideband harmonics will be zero.
+ The sideband hamonics center around the frequency of kNf_c (k = 1, 2, ..., ∞).

Eq. (18) expresses for an ideal line-to-line output voltage without considering the voltage drop on arm inductor. However, there is still a voltage drop on arm inductor in practice. Thus, the effect of arm inductor should be taken in account. From Fig. 1, if the AC grid is replaced by a series RL load, the output voltage and current of the MMC will be described by

$$i_j = i_{uj} - i_{lj} \tag{19}$$

$$v_{tj} = i_j Z = i_j \left(R_1 + j\omega_0 \left(L + L_1\right)\right) \tag{20}$$

$$v_j = \frac{v_{lj} - v_{uj}}{2} \tag{21}$$

$$v_{tj} = -L_0 \frac{di_{uj}}{dt} + \frac{V_{dc}}{2} - v_{uj} \tag{22}$$

$$v_{tj} = L_0 \frac{di_{lj}}{dt} - \frac{V_{dc}}{2} + v_{lj} \tag{23}$$

where $j = a, b, c$ denotes phase A, B, and C, respectively. v_{tj} is the real phase output voltage of phase j that is considering the effect of arm inductor.

By adding (22) and (23), we can obtain

$$\frac{v_{lj} - v_{uj}}{2} = \frac{L_0}{2} \frac{di_j}{dt} + v_{tj} \tag{24}$$

Substituting (20) and (21) into (24), the ideal phase output voltage can be expressed as

$$v_j = \frac{L_0}{2} \frac{di_j}{dt} + i_j \left(R_1 + j\omega_0 \left(L + L_1\right)\right) \tag{25}$$

From (25), an equivalent circuit of the MMC is given in Fig. 4.

Assuming that PWM converter generates the harmonics into the output voltage and current. We have (26) and (27).

$$i_j = \sum_{h=1}^{\infty} i_{jh} \tag{26}$$

$$v_j = \sum_{h=1}^{\infty} v_{jh} \tag{27}$$

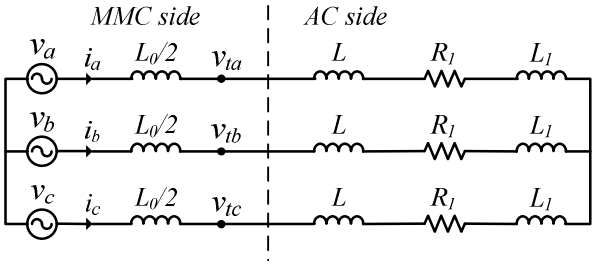

Fig. 4. Equivalent circuit of the MMC

At a steady-state, the harmonic currents can be calculated as

$$i_{jh} = \frac{v_{jh}}{Z_1} = \frac{v_{jh}}{R_1 + j\omega_h\left(\frac{L_0}{2} + L + L_1\right)} \tag{28}$$

where h is the harmonic order, h = 2, 3, ..., ∞ and $\omega_h = 2\pi f_0 h$.

Thus, the harmonic components of real phase and line-to-line voltages will be expressed as

$$v_{tjh} = v_{jh} - i_{jh}\left(j\frac{\omega_h L_0}{2}\right) \tag{29}$$

$$v_{tabh} = v_{tah} - v_{tbh} \tag{30}$$

4. Simulation Results and Discussion

In order to analyze harmonics in the MMC by using DFS, several calculations and simulations will be performed in Matlab programming and PSCAD/EMTDC simulation program. The parameters of the MMC are given in Table 1. In this table, some parameters such as carrier frequency, number of SMs per arm and SM capacitance will be changed according to the analytical objectives.

4.1 Verification of DFS algorithm

This section is to verify the DFS algorithm in Section 3. The carrier frequency, number of SMs per arm and modulation index are set to 360 Hz, 10 and 0.8165, respectively.

Fig. 5 shows a comparison between the analytical results of using the DFS and the simulation results of using the FFT. As seen in Figs. 5(a) and (b), two algorithms can bring to the same results. The THDs obtained by using DFS and FFT are 8.23% and 8.07%, respectively. The THD error between two algorithms is not significant. Therefore, the precision of the DFS algorithm is confirmed. The total switching frequency is 3600 Hz (f_{ct} = 3600 Hz) that is corresponding to 60th harmonic order. In the line-to-line voltage, there are no baseband harmonics, carrier harmonics, the sideband harmonics with even combinations of 10.m + n and triplen sideband harmonics of h.3th (h=1,2,..., ∞). The sideband harmonics are centered around the harmonic order of k.60th (k = 1, 2, ..., ∞). These results exactly match the theoretical analysis in Section 3.

Table 1. The parameters of MMC

Quantity	Value
Active power (P)	20 MW
Reactive power (Q)	15 MVar
AC voltage (V_s)	22.9 kV
Fundamental frequency (f_0)	60 Hz
Carrier frequency (f_c)	According to analysis
Transformer ratio	22.9 kV/12 kV
DC-link voltage (V_{dc})	24 kV
Number of SMs per arm (N)	According to analysis
Arm inductance (L_0)	3 mH
SM capacitance (C)	7000 µF
Modulation index (M)	According to analysis

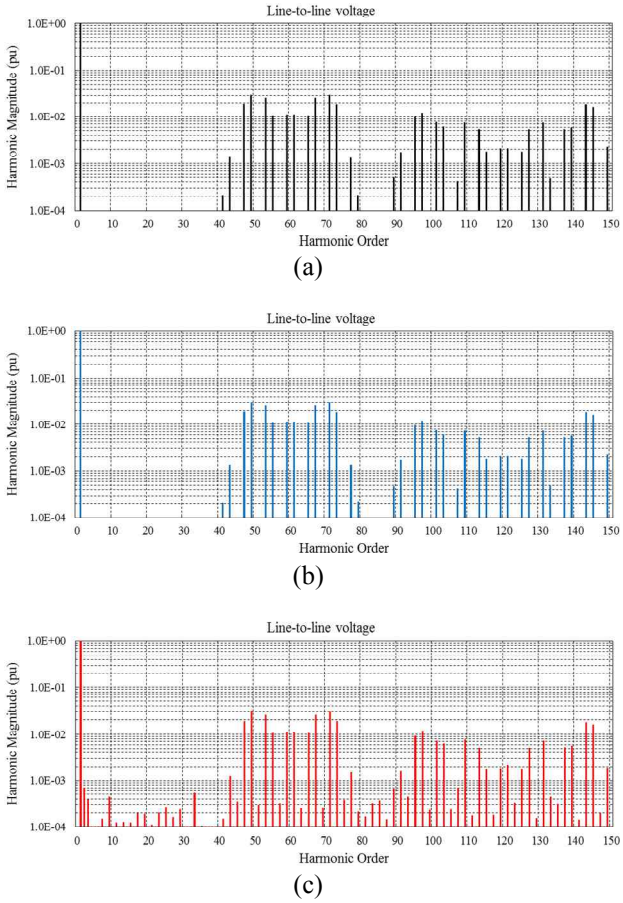

Fig. 5. Analytical results and simulation results: (a) Analytical results, (b) Simulation results with simulation time step of 0.5 µs, (c) Simulation results with simulation time step of 10 µs

The harmonic spectrum of using the FFT significantly depends on the simulation time step. With the simulation time step of 10 µs, the simulation results showed in Fig. 5(c) contains some harmonics (smaller than 10^{-3}) that do not exist in the analytical results or in the simulation results

Table 2. THDs of the ideal and real line-to-line voltages

	THD (%)
Ideal line-to-line voltage	12.14
Real line-to-line voltage	8.23

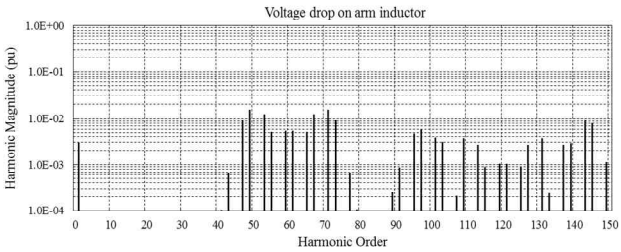

Fig. 6. Voltage drop on arm inductor

obtained by using the simulation time step of 0.5 μs as shown in Fig. 5(b). However, the executive time of simulation results in Fig. 5(b) is extremely long. This explains the usefulness of the DFS in this study.

The voltage drop on arm inductor is shown in Fig. 6. It is calculated by subtracting the real line-to-line voltage in (30) from the ideal line-to-line voltage in (18). There is a voltage drop on arm inductor that leads a difference between the ideal and real voltages. This can be explained by assuming that the harmonic components in the arm currents are sinusoidal waveforms and there are no dc components. Thus, there exists an impedance across the arm inductor and causes a voltage drop on this impedance. The THD of ideal and real voltages is shown in Table 2. There is a large difference in THD between two voltages. Thus, the voltage drop on arm inductor must be considered whenever calculating harmonics in the MMC.

4.2 Harmonics versus number of levels of MMC

In this section, the number of SMs per arm will be changed in order to analyze the distribution of harmonics versus number of levels of MMC. The analytical results are shown in Fig. 7. The modulation index is the same with Section 4.1. The carrier frequencies are 900 Hz, 360 Hz and 180 Hz corresponding to 5-level, 11-level and 21-level MMCs, respectively. These carrier frequencies ensure that the total switching frequencies are the same in three cases, f_{ct} = 3600 Hz. With the higher number of levels of MMC, the sideband harmonic region is wider while the magnitude of harmonics is smaller. This leads a distribution of THD in three cases as shown in Fig. 8. There is an error in the THD between the analytical results and the simulation results, but this error is not significant. The increasing series of THDs is 21-level MMC (3.7%), 11-level MMC (8.23%) and 5-level MMC (19.76%). In other words, the higher number of levels of MMC can achieve a lower THD. This will be explained as follows. If the number of levels of the MMC increases, the output voltage will be more nearly sinusoidal waveform. Thus, the harmonics and THD will be decreased.

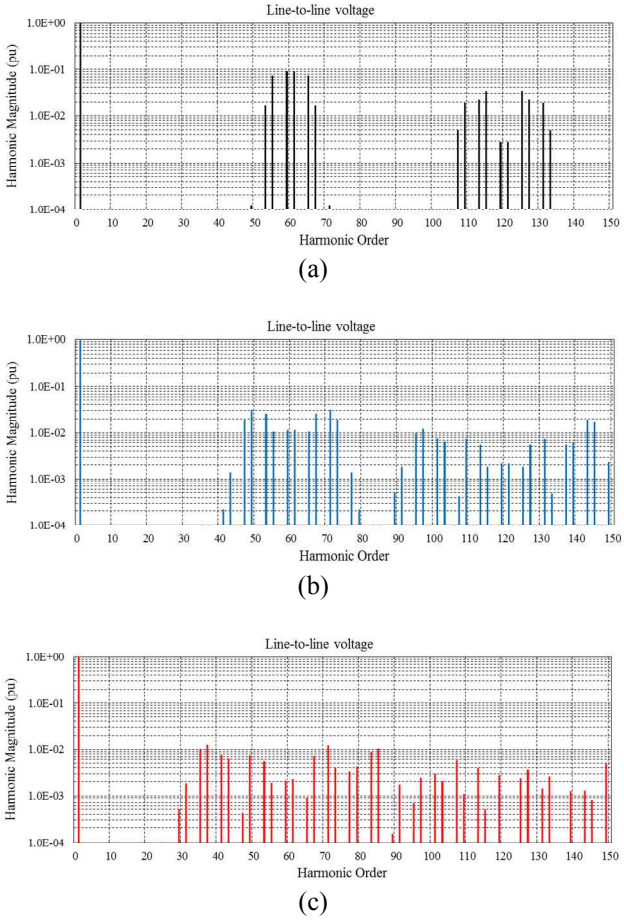

Fig. 7. Distribution of harmonics versus number of levels of MMC (f_{ct} = 3600 Hz). (a) 5-level MMC, (b) 11-level MMC, (c) 21-level MMC

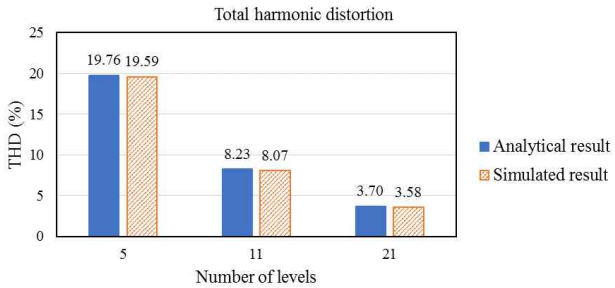

Fig. 8. Total harmonic distortion versus number of levels of MMC

4.3 Harmonics versus total switching frequency

In this section, number of SMs per arm and modulation index are 10 and 0.8165, respectively. The carrier frequencies are 180 Hz, 360 Hz and 540 Hz. The distribution of harmonics versus total switching frequency are shown in Fig. 9. The sideband harmonics will be displaced to higher frequency region if the total switching frequency increases,

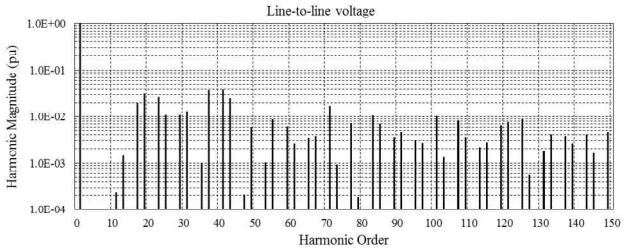

(a)

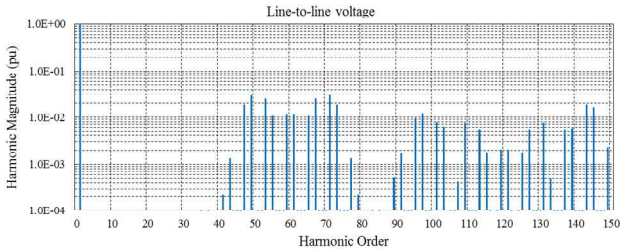

(b)

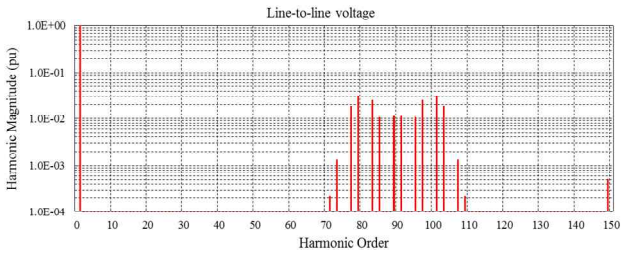

(c)

Fig. 9. Distribution of harmonics versus total switching frequency (11-level MMC): (a) f_{ct} = 1800 Hz, (b) f_{ct} = 3600 Hz, (c) f_{ct} = 5400 Hz

as seen in Figs. 9(a)-(c). This is due to the center frequency of the harmonics is higher and the sideband harmonics only focus around the center frequency. The THD versus total switching frequency is shown in Fig. 10. The THD is slightly reduced with an increase in the total switching frequency. The THD corresponding to the total switching frequency of 1800 Hz is about 8.88%. If the total switching frequency is double time (3600 Hz) and triple time (5400 Hz), the THD will be about 8.23% and 8.0%, respectively.

4.4 Harmonics versus modulation index

The analytical conditions are carrier frequency of 360 Hz and number of SMs per arm of 10. In this paper, the modulation index must be higher than 0.8 to ensure number of levels in output voltage equal to 11 levels. The analytical results are shown in Fig. 11. If the modulation index is smaller than 1.0, the magnitude of the output voltage is linear to the modulation index and it is illustrated by a blue curves in Fig. 11. However, the change of THD is not linear to the modulation index (orange curves in Fig. 11). The THD is smaller with a higher modulation index

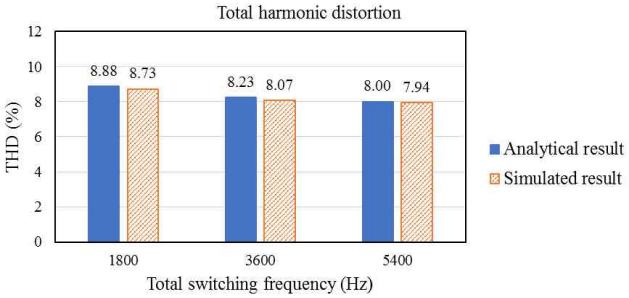

Fig. 10. Total harmonic distortion versus total switching frequency

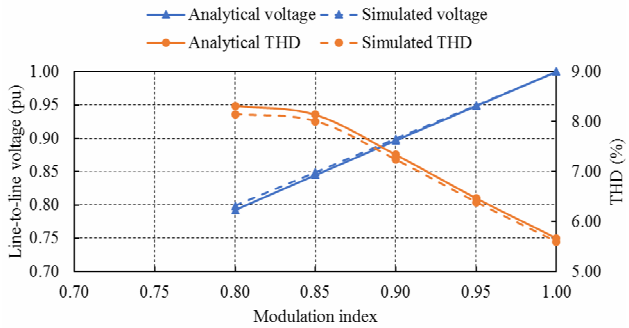

Fig. 11. Harmonic profile of 11-level MMC

because the fundamental component of the output voltage increases along with the modulation index.

5. Conclusion

This paper has presented a harmonic analysis of the MMC using the DFS algorithm. Considering the effect of arm inductor, the analytical results of using the DFS has been confirmed by comparing with the simulation results of using the FFT. This means that the DFS can be used to analyze the harmonics in the MMC. The MMC with higher number of levels can reduce the THD in the output voltage significantly. In this case, the bandwidth of harmonics is wider, but the magnitude of harmonics is smaller. The THD can be only reduced slightly if the total switching frequency increases. The increase in total switching frequency will displace harmonics to higher frequency region where the harmonics can be removed easily by using filter. Besides, the relationship between the THD and the modulation index is also researched in this paper. The results show that the THD will be lower if the modulation index increases. These conclusions play an important role in design as well as operation in order to reduce harmonics of the MMC.

Acknowledgements

This work was supported by the Korea Institute of

Energy Technology Evaluation and Planning (KETEP) and the Ministry of Trade, Industry & Energy (MOTIE) of the Republic of Korea (No. 20173010024890).

This work was supported by the Korea Institute of Energy Technology Evaluation and Planning (KETEP) and the Ministry of Trade, Industry & Energy (MOTIE) of the Republic of Korea (No. 20174030201490).

References

[1] S. Allebrod, R. Hamerski, and R. Marquardt, "New Transformerless, Scalable Modular Multilevel Converters for HVDC-Transmission," *IEEE Power Electronics Specialists Conference*, PESC 2008, pp. 174-179, 2008.

[2] S. Rohner, S. Bernet, M. Hiller, and R. Sommer, "Modulation, Losses, and Semiconductor Requirements of Modular Multilevel Converters," *IEEE Transactions on Industrial Electronics*, vol. 57, no. 8, pp. 2633-2642, Aug. 2010.

[3] Qingrui Tu, Zheng Xu, and Lie Xu, "Reduced Switching-Frequency Modulation and Circulating Current Suppression for Modular Multilevel Converters," *IEEE Transactions on Power Delivery*, vol. 26, no. 3, pp. 2009-2017, July 2011.

[4] M. Saeedifard and R. Iravani, "Dynamic Performance of a Modular Multilevel Back-to-Back HVDC System," *IEEE Transactions on Power Delivery*, vol. 25, no. 4, pp. 2903-2912, Oct. 2010.

[5] Ngoc-Thinh Quach, Ji-Han Ko, Dong-Wan Kim, and Eel-Hwan Kim, "An Application of Proportional-Resonant Controller in MMC-HVDC System under Unbalanced Voltage Conditions," *Journal of Electrical Engineering & Technology*, vol. 9, no. 5, pp. 1746-1752, Sept. 2014.

[6] G. S. Konstantinou and V. G. Agelidis, "Performance Evaluation of Half-Bridge Cascaded Multilevel Converters Operated with Multicarrier Sinusoidal PWM Techniques, *4th IEEE Conference on Industrial Electronics and Applications*, 2009. ICIEA 2009, pp. 3399-3404, May 2009.

[7] G. Carrara, S. Gardella, M. Marchesoni, R. Salutari, and G. Sciutto, "A New Multilevel PWM Method: A Theoretical Analysis, *IEEE Transactions on Power Electronics*, vol. 7, no. 3, pp. 497-505, Jul. 1992.

[8] A. K. Gupta and A. M. Khambadkone, "A Space Vector PWM Scheme for Multilevel Inverters Based on Two-Level Space Vector PWM, *IEEE Transactions on Industrial Electronics*, vol. 53, no. 5, pp. 1631-1639, Oct. 2006.

[9] M. Guan, Z. Xu, and H. Chen, "Control and Modulation Strategies for Modular Multilevel Converter Based HVDC System, *IECON 2011 - 37th Annual Conference on IEEE Industrial Electronics Society*, pp. 849-854, Nov. 2011.

[10] D. Grahame Holmes and Thomas A. Lipo, "Pulse Width Modulation for Power Converters - Principles and Practice" *Wiley-IEEE Press*, 2003.

[11] W. R. Bennett, "New Results in the Calculation of Modulation Products," *The Bell System Technical Journal*, vol. 12, pp. 228-243, April 1933.

[12] Milijana Odavic, Mark Sumner, Pericle Zanchetta, and Jon C. Clare, "A Theoretical Analysis of the Harmonic Content of PWM Waveforms for Multiple-Frequency Modulators," *IEEE Transactions on Power Electronics*, vol. 25, no. 1, pp. 131-141, Jan. 2010.

[13] Gary. W. Chang, Shin-Kuan Chen, Huai-Jhe Su, and Ping-Kuei Wang, "Accurate Assessment of Harmonic and Interharmonic Currents Generated by VSI-Fed Drives under Unbalanced Supply Voltages," *IEEE Transactions on Power Delivery*, vol. 26, no. 2, pp. 1083-1091, April 2011.

[14] Zhonghui Bing and Jian Sun, "Frequency-Domain Modeling of Multipulse Converters by Double-Fourier Series Method," *IEEE Transactions on Power Electronics*, vol. 26, no. 12, pp. 3804-3809, Dec. 2011.

[15] C. M. Wu, Wing-Hong Lau, and Henry Shu-Hung Chung, "Analytical Technique for Calculating the Output Harmonics of an H-Bridge Inverter with Dead Time," *IEEE Transactions on Circuits and Systems*, vol. 46, no. 5, pp. 617-627, May 1999.

Ngoc-Thinh Quach He received B.S. degree in Electrical Engineering from Can Tho University, Vietnam, in 2007, M.S. and PhD. degrees in Electrical Engineering from Jeju National University, S. Korea, in 2012 and 2015, respectively. Since 2015, he has been with the Department of Electrical Engineering, Can Tho University in Can Tho city, Viet Nam, where he is currently a lecturer. He was a postdoctoral researcher at Jeju National University in 2016. His research interests include power electronics, renewable energy systems, HVDC systems, and power system stability.

Sang Heon Chae He received a B.S. degree in Electrical Engineering from Jeju National University, S. Korea, in 2015. He is currently a Ph.D. student in the Department of Electrical Engineering, Jeju National University, S. Korea. His research interests include wind energy systems, BESS system, and power electronics.

Jin Hong Ahn He received a B.S. and M.S. degree in Electrical Engineering from Jeju National University, S. Korea, in 2009 and 2011, respectively. He is currently a Ph.D. student in the Department of Electrical Engineering, Jeju National University, S. Korea. His research interests include wind energy systems, STATCOM, and power electronics.

Eel-Hwan Kim He received his B.S., M.S. and Ph.D. degrees in Electrical Engineering from Chung-Ang University, Seoul, Korea, in 1985, 1987 and 1991, respectively. Since 1991, he has been with the Department of Electrical Engineering, Jeju National University in Jeju, Korea, where he is currently a professor. He was a Visiting Scholar at the Ohio State University in 1995 and University of Washington in 2004. His research activities are in the area of power electronics and control, which includes the drive system, renewable energy control applications, and power quality. He is a member of KIEE, KIPE, and IEEE.